

# Using an Anti-Relaxation Step to Improve the Accuracy of the Frictional Contact Solution in a DVI Framework for Rigid Body Dynamics

Daniel Melanz<sup>a</sup>, Hammad Mazhar<sup>a</sup>, Dan Negrut<sup>a,\*</sup>

<sup>a</sup>*Department of Mechanical Engineering, University of Wisconsin-Madison, Madison, WI 53706-1572, USA*

---

## Abstract

Systems composed of rigid bodies interacting through frictional contact are manifest in several science and engineering problems. The number of contacts can be small, such as in robotics and geared machinery, or large, such as in terramechanics applications, additive manufacturing, farming, food industry, and pharmaceutical industry. Currently, there are two popular approaches for handling the frictional contact problem in dynamic systems. The penalty method calculates the frictional contact force based on the kinematics of the interaction, some representative parameters, and an empirical force law. Alternatively, the complementarity method, based on a differential variational inequality (DVI), enforces non-penetration of rigid bodies via a complementarity condition. This contribution concentrates on the latter approach and investigates the impact of an anti-relaxation step that improves the accuracy of the frictional contact solution. We show that the proposed anti-relaxation step incurs a relatively modest cost to improve the quality of a numerical solution strategy which poses the calculation of the frictional contact forces as a cone-complementarity problem.

---

## 1. Introduction

Nonsmooth rigid multibody dynamics (NRMD) consists of predicting the position and velocity evolution of a group of rigid particles that are subject to non-interpenetration, collision, adhesion, and dry friction constraints and to possibly global forces (such as electrostatic and gravitational forces). The dynamics of such a group of particles is nonsmooth because of the intermittent nature of non-interpenetration, collision, and adhesion constraints and because of the nonsmooth nature of the dry friction constraints at stick-slip transitions. Using Coulomb's Law of Friction, the dynamics of such a nonsmooth rigid multibody system can be resolved by simultaneously solving a linear complementarity problem (LCP) that links the normal contact impulses to the distances between bodies and a quadratic minimization problem that links the normal and tangential contact impulses via conic constraints. Solving this coupled system, or differential variational inequality (DVI), has proven to be quite difficult although polyhedral linearizations of the minimization problem have provided a reasonable approximation. To circumvent the difficulties posed by increasing complexity of classical LCP solvers and the increased size and inaccuracy introduced by polyhedral approximation, however, a novel solution method was developed based on a fixed-point iteration with projection on a convex set, that can directly solve large cone complementarity problems with low computational overhead. This solution method works by adding a relaxation term to transform the original problem into a cone complementarity problem (CCP). By considering the Karush-Kuhn-Tucker (KKT) conditions, the CCP is further transformed into a cone-constrained quadratic optimization problem (CCQO) for which several iterative solution methods exist. In the DVI method, a CCQO must be solved at each time step of the simulation, where the unknowns are the normal and frictional contact forces between interacting bodies. The time-stepping scheme was proven to converge in a measure differential inclusion sense, to the solution

---

\*Corresponding author.

Email addresses: [melanz@wisc.edu](mailto:melanz@wisc.edu) (Daniel Melanz), [mazhar@wisc.edu](mailto:mazhar@wisc.edu) (Hammad Mazhar), [negrut@wisc.edu](mailto:negrut@wisc.edu) (Dan Negrut)

of the original continuous-time DVI. This paper uses an iterative refinement scheme, called anti-relaxation, to update the objective function of the CCQO to yield a optimum that is equivalent to the solution of the original NRMD problem.

## 2. Modeling frictional contact via DVI

Consider a three dimensional (3D) system of rigid bodies which may interact through frictional contact. An absolute Cartesian coordinate system will be used to define the equations of motion for the time evolution of such a system [1]. Therefore, the generalized positions  $\mathbf{q} = [\mathbf{r}_1^T, \epsilon_1^T, \dots, \mathbf{r}_{n_b}^T, \epsilon_{n_b}^T]^T$  and their time derivatives  $\dot{\mathbf{q}} = [\dot{\mathbf{r}}_1^T, \dot{\epsilon}_1^T, \dots, \dot{\mathbf{r}}_{n_b}^T, \dot{\epsilon}_{n_b}^T]^T$  are used to describe the state of the system. Here,  $\mathbf{r}_j$  is the absolute position of the center of mass of body  $j$  and  $\epsilon_j$  is the quaternion used to represent rotation. Note that the angular velocity of body  $j$  in local coordinates,  $\bar{\omega}_j$ , may be used in place of the time derivative of the rotation quaternion. Then, the vector of generalized velocities  $\mathbf{v} = [\dot{\mathbf{r}}_1^T, \bar{\omega}_1^T, \dots, \dot{\mathbf{r}}_{n_b}^T, \bar{\omega}_{n_b}^T]^T$  can be related to  $\dot{\mathbf{q}}$  via a linear mapping given as  $\dot{\mathbf{q}} = \mathbf{T}(\mathbf{q})\mathbf{v}$  [1].

Due to the rigid body assumption and the choice of centroidal reference frames, the generalized mass matrix  $\mathbf{M}$  is constant and diagonal. Further, let  $\mathbf{f}(t, \mathbf{q}, \mathbf{v})$  be a set of generalized external forces which act on the bodies in the system. Finally, the second order differential equations which govern the time evolution of the system can be written in the matrix form  $\mathbf{M}\ddot{\mathbf{v}} = \mathbf{f}(t, \mathbf{q}, \mathbf{v})$  [2].

The rigid body assumption implies that elements that come into contact should not penetrate each other. Such a condition is enforced here through unilateral constraints. To enforce the non-penetration constraint, a gap function,  $\Phi(\mathbf{q}, t)$ , must be defined for each pair of near-enough bodies. When two bodies are in contact, or  $\Phi(\mathbf{q}, t) = 0$ , a normal force acts on each of the two bodies at the contact point. When a pair of bodies is not in contact, or  $\Phi(\mathbf{q}, t) > 0$ , no normal force exists. This captures a complementarity condition, where one of two scenarios must hold. Either the gap is positive and the normal force is exactly zero, or vice-versa: the gap is zero, and the normal force is positive.

When a pair of bodies is in contact, friction forces may be introduced into the system through the Coulomb friction model [3]. The force associated with contact  $i$  can then be decomposed into the normal component,  $\mathbf{F}_{i,N} = \hat{\gamma}_{i,n} \mathbf{n}_i$ , and the tangential component,  $\mathbf{F}_{i,T} = \hat{\gamma}_{i,u} \mathbf{u}_i + \hat{\gamma}_{i,w} \mathbf{w}_i$ , where multipliers  $\hat{\gamma}_{i,n} > 0$ ,  $\hat{\gamma}_{i,u}$ , and  $\hat{\gamma}_{i,w}$  represent the magnitude of the force in each direction,  $\mathbf{n}_i$  is the normal direction at the contact point, and  $\mathbf{u}_i$  and  $\mathbf{w}_i$  are two vectors in the contact plane such that  $\mathbf{n}_i$ ,  $\mathbf{u}_i$ , and  $\mathbf{w}_i$  are mutually orthonormal. The governing differential equations are obtained by combining the rigid body dynamics equations with the unilateral constraint equations. Then, the governing differential equations, which assume the form of a differential variational inequality (DVI) problem, become [4],

$$\dot{\mathbf{q}} = \mathbf{T}(\mathbf{q})\mathbf{v} \quad (1)$$

$$\mathbf{M}(\mathbf{q})\ddot{\mathbf{v}} = \mathbf{f}(t, \mathbf{q}, \mathbf{v}) + \sum_{i=1}^{N_c} (\hat{\gamma}_{i,n} \mathbf{D}_{i,n}^T + \hat{\gamma}_{i,u} \mathbf{D}_{i,u}^T + \hat{\gamma}_{i,w} \mathbf{D}_{i,w}^T) \quad (2)$$

$$0 \leq \Phi_i(\mathbf{q}, t) \perp \hat{\gamma}_{i,n} \geq 0 \quad i = 1, 2, \dots, N_c \quad (3)$$

$$(\hat{\gamma}_{i,u}, \hat{\gamma}_{i,w}) = \arg \min_{\sqrt{\gamma_{i,u}^2 + \gamma_{i,w}^2} \leq \mu_i \hat{\gamma}_{i,n}} (\gamma_{i,u} \mathbf{v}^T \mathbf{D}_{i,u} + \gamma_{i,w} \mathbf{v}^T \mathbf{D}_{i,w}) . \quad (4)$$

The tangent space generators  $\mathbf{D}_i = [\mathbf{D}_{i,n}, \mathbf{D}_{i,u}, \mathbf{D}_{i,w}] \in \mathbb{R}^{6n_b \times 3}$  are defined as

$$\mathbf{D}_i^T = [\mathbf{0}, \dots, -\mathbf{A}_{i,p}^T, \mathbf{A}_{i,p}^T \mathbf{A}_A \tilde{\mathbf{s}}_{i,A}, \mathbf{0}, \dots, \mathbf{0}, \mathbf{A}_{i,p}^T, -\mathbf{A}_{i,p}^T \mathbf{A}_B \tilde{\mathbf{s}}_{i,B}, \dots, \mathbf{0}] , \quad (5)$$

and are used to transform the contact forces from local to global frame,  $\mu_i$  is the coefficient of friction for contact  $i$ , and  $N_c$  is the total number of possible contacts. Note that for contact between bodies  $A$  and  $B$ , the matrix  $\mathbf{A}_{i,p} = [\mathbf{n}_i, \mathbf{u}_i, \mathbf{w}_i] \in \mathbb{R}^{3 \times 3}$  is used to represent the orientation of the contact in global coordinates, and the matrices  $\mathbf{A}_A$  and  $\mathbf{A}_B$  as the rotation matrices of bodies  $A$  and  $B$ , respectively.

## 2.1. The numerical solution scheme

Equations 1 through 4 are discretized to obtain an approximation of the solution at discrete instants in time. In the following, superscript  $(l)$  denotes a variable at time instant  $t^{(l)}$ . For example,  $\mathbf{q}^{(l)}$  and  $\mathbf{v}^{(l)}$  represent the position and velocity at time  $t^{(l)}$ , respectively. Further,  $\gamma_i = h\hat{\gamma}_i$  is the contact impulse for contact  $i$ . Then, the discretized form of the equations of motion is posed as [5]:

$$\mathbf{q}^{(l+1)} = \mathbf{q}^{(l)} + h\mathbf{T}\left(\mathbf{q}^{(l)}\right)\mathbf{v}^{(l+1)} \quad (6)$$

$$\mathbf{M}\left(\mathbf{v}^{(l+1)} - \mathbf{v}^{(l)}\right) = h\mathbf{f}\left(t^{(l)}, \mathbf{q}^{(l)}, \mathbf{v}^{(l)}\right) + \sum_{i=1}^{N_c} (\gamma_{i,n}\mathbf{D}_{i,n}^T + \gamma_{i,u}\mathbf{D}_{i,u}^T + \gamma_{i,w}\mathbf{D}_{i,w}^T) \quad (7)$$

$$0 \leq \frac{1}{h}\Phi_i\left(\mathbf{q}^{(l)}, t\right) + \mathbf{D}_{i,n}^T\mathbf{v}^{(l+1)} \perp \gamma_{i,n} \geq 0, \quad i = 1, 2, \dots, N_c \quad (8)$$

$$(\gamma_{i,u}, \gamma_{i,w}) = \arg \min_{\sqrt{\gamma_{i,u}^2 + \gamma_{i,w}^2} \leq \mu_i \gamma_{i,n}} \left( \gamma_{i,u}\mathbf{v}^{(l+1)T}\mathbf{D}_{i,u} + \gamma_{i,w}\mathbf{v}^{(l+1)T}\mathbf{D}_{i,w} \right), \quad (9)$$

where  $t^{(l+1)} = t^{(l)} + h$  for some integration time step  $h$ . Methods for solving the above problem in the most general case are lacking and various strategies are employed to simplify it [6]. For example, the friction cones can be approximated by linear faceted pyramids, leading to a linear complementarity problem (LCP) which can be solved by pivoting or simplex methods [7]. However, these approaches in the class of direct methods can have exponential complexity in the worst-case [8]. Another artifact is the lack of isotropy, given that the friction cone is approximated by a pyramid. An alternative is to introduce a relaxation to the complementarity constraints, replacing  $0 \leq \left(\frac{1}{h}\Phi_i\left(\mathbf{q}^{(l)}, t\right) + \mathbf{D}_{i,n}^T\mathbf{v}^{(l+1)}\right) \perp \gamma_{i,n} \geq 0$  with the following [9]:

$$0 \leq \left( \frac{1}{h}\Phi_i\left(\mathbf{q}^{(l)}, t\right) + \mathbf{D}_{i,n}^T\mathbf{v}^{(l+1)} - \mu_i \sqrt{(\mathbf{D}_{i,u}^T\mathbf{v}^{(l+1)})^2 + (\mathbf{D}_{i,w}^T\mathbf{v}^{(l+1)})^2} \right) \perp \gamma_{i,n} \geq 0. \quad (10)$$

As seen from Eq. 10, the modification is small when  $\mu$  or the relative tangential velocity at the point of contact,  $\sqrt{(\mathbf{D}_{i,u}^T\mathbf{v}^{(l+1)})^2 + (\mathbf{D}_{i,w}^T\mathbf{v}^{(l+1)})^2}$ , are small. Additionally, it has been shown in [5] that the solution of the modified scheme will still approach the solution of the original problem as the step-size tends to zero. An iterative method has been developed to solve this problem [10, 11]. It can be shown that solving the relaxed discretized equations of motion is equivalent to solving a Cone Complementarity Problem (CCP) of the form

$$\begin{aligned} & \text{Find } \gamma_i^{(l+1)}, \text{ for } i = 1, \dots, N_c \\ & \text{such that } \Upsilon_i \ni \gamma_i^{(l+1)} \perp -\left(\mathbf{N}\gamma^{(l+1)} + \mathbf{r}\right)_i \in \Upsilon_i^\circ \\ & \text{where } \Upsilon_i = \{[x, y, z]^T \in \mathbb{R}^3 | \sqrt{y^2 + z^2} \leq \mu_i x\} \\ & \text{and } \Upsilon_i^\circ = \{[x, y, z]^T \in \mathbb{R}^3 | x \leq -\mu_i \sqrt{y^2 + z^2}\}, \end{aligned} \quad (11)$$

with matrix  $\mathbf{N}$  and vector  $\mathbf{r}$  defined as

$$\mathbf{N} = \mathbf{D}^T \mathbf{M}^{-1} \mathbf{D}, \quad (12)$$

$$\mathbf{r} = \mathbf{b} + \mathbf{D}^T \mathbf{M}^{-1} \mathbf{k}, \quad (13)$$

where  $\mathbf{b}^T = [\mathbf{b}_1^T, \dots, \mathbf{b}_{N_c}^T]$  with  $\mathbf{b}_i = \left[\frac{1}{h}\Phi_i, 0, 0\right]^T \in \mathbb{R}^3$ , and  $\mathbf{k} = \mathbf{M}\mathbf{v}^{(l)} + h\mathbf{f}(t^{(l)}, \mathbf{q}^{(l)}, \mathbf{v}^{(l)})$ .

It can be verified by considering the KKT first-order necessary conditions that solving the CCP of Eq. 11 is equivalent to solving a cone-constrained quadratic optimization (CCQO) problem. For the case with only unilateral constraints (contacts), this optimization problem takes the form [12, 13],

$$\begin{aligned} \min \mathbf{q}(\gamma) &= \frac{1}{2} \gamma^T \mathbf{N} \gamma + \mathbf{r}^T \gamma \\ \text{subject to } \gamma_i &\in \Upsilon_i \text{ for } i = 1, 2, \dots, N_c, \end{aligned} \quad (14)$$

where  $\gamma_i$  is the triplet of multipliers associated with contact  $i$  and  $\Upsilon_i$  is the friction cone of contact  $i$ . Note also that  $\gamma = [\gamma_1^T, \gamma_2^T, \dots, \gamma_{N_c}^T]^T$ .

It should be noted that the relaxation introduced by Eq. 10 is non-physical. The objective function of the CCQO can be modified by an anti-relaxation term,  $\mathbf{a}^T = [\mathbf{a}_1^T, \dots, \mathbf{a}_{N_c}^T]$  with  $\mathbf{a}_i = [\alpha_i, 0, 0]^T \in \mathbb{R}^3$ , to result in a solution that is equivalent to the optimum of Eqs. 1-4. This modification results in the anti-relaxed CCQO,

$$\begin{aligned} \min \mathbf{q}(\gamma) &= \frac{1}{2} \gamma^T \mathbf{N} \gamma + (\mathbf{r} + \mathbf{a})^T \gamma \\ \text{subject to } \gamma_i &\in \Upsilon_i \text{ for } i = 1, 2, \dots, N_c, \end{aligned} \quad (15)$$

The value of  $\alpha$  can be determined by considering the Lagrangian,  $\mathcal{L}(\gamma, \lambda)$ , for the constrained optimization problem in Eq. 15,

$$\mathcal{L}(\gamma, \lambda) = \frac{1}{2} \gamma^T \mathbf{N} \gamma + (\mathbf{r} + \mathbf{a})^T \gamma - \sum_{i=1}^{N_c} \lambda_i \left( \mu_i \gamma_{i,n} - \sqrt{\gamma_{i,u}^2 + \gamma_{i,w}^2} \right). \quad (16)$$

Then, the KKT conditions for Eq. 15 can be stated as follows. If  $\gamma^*$  is a local solution of Eq. 15, then there exists a vector  $\lambda^*$  of Lagrange multipliers,  $\lambda_i^*, i = 1, \dots, N_c$ , such that the following conditions are satisfied,

$$\nabla \mathcal{L}(\gamma^*, \lambda^*) = 0, \quad (17)$$

$$c_i(\gamma^*) \geq 0, \quad \forall i = 1, \dots, N_c \quad (18)$$

$$\lambda_i^* \geq 0, \quad \forall i = 1, \dots, N_c \quad (19)$$

$$\lambda_i^* c_i(\gamma^*) = 0, \quad \forall i = 1, \dots, N_c \quad (20)$$

where  $c_i(\gamma) = \mu_i \gamma_{i,n} - \sqrt{\gamma_{i,u}^2 + \gamma_{i,w}^2}$ . These equations can be stated in a more manageable form by defining the vector  $\mathbf{s}$  as follows:

$$\mathbf{s} = \left[ \dots, \lambda_i \mu_i, \frac{-\lambda_i \gamma_{i,u}}{\sqrt{\gamma_{i,u}^2 + \gamma_{i,w}^2}}, \frac{-\lambda_i \gamma_{i,w}}{\sqrt{\gamma_{i,u}^2 + \gamma_{i,w}^2}}, \dots \right]^T \in \mathbb{R}^{3N_c} \quad (21)$$

Then, the condition in Eq. 17 can be expressed as follows:

$$\mathbf{N} \gamma + \mathbf{r} + \mathbf{a} = \mathbf{s} \quad (22)$$

$$\mathbf{D}^T \mathbf{M}^{-1} \mathbf{D} \gamma + \mathbf{D}^T \mathbf{M}^{-1} \mathbf{k} + \mathbf{b} + \mathbf{a} = \mathbf{s} \quad (23)$$

$$\mathbf{D}^T \mathbf{M}^{-1} (\mathbf{D} \gamma) + \mathbf{b} + \mathbf{a} = \mathbf{s} \quad (24)$$

$$\mathbf{D}^T \mathbf{v} + \mathbf{b} + \mathbf{a} = \mathbf{s} \quad (25)$$

Specifically, the rows of Eq. 22 associated with contact  $i$  are

$$(\mathbf{N}\gamma + \mathbf{r} + \mathbf{a})_i = \mathbf{D}_i^T \mathbf{v} + \mathbf{b}_i + \mathbf{a}_i = \mathbf{s}_i \quad (26)$$

$$\begin{bmatrix} \mathbf{D}_{i,n}^T \mathbf{v} + \frac{1}{h} \Phi_i + \alpha_i \\ \mathbf{D}_{i,u}^T \mathbf{v} \\ \mathbf{D}_{i,w}^T \mathbf{v} \end{bmatrix} = \begin{bmatrix} \lambda_i \mu_i \\ \frac{-\lambda_i \gamma_{i,u}}{\sqrt{\gamma_{i,u}^2 + \gamma_{i,w}^2}} \\ \frac{-\lambda_i \gamma_{i,w}}{\sqrt{\gamma_{i,u}^2 + \gamma_{i,w}^2}} \end{bmatrix}. \quad (27)$$

For the case where  $\gamma_{i,n} > 0$ , the quantity in the first line of Eq. 27 must be equal to zero according to Eq. 8 and  $\alpha_i = \lambda_i \mu_i$ . By manipulating the second and third lines of Eq. 27,  $\lambda_i$  can be expressed as follows:

$$\lambda_i = \sqrt{(\mathbf{D}_{i,u}^T \mathbf{v})^2 + (\mathbf{D}_{i,w}^T \mathbf{v})^2} \quad (28)$$

## 2.2. Anti-relaxation via iterative refinement

As the anti-relaxation term  $\alpha_i$  relies on the value of  $\mathbf{v}^{(l+1)}$ , the approximation  $\mathbf{v}_k = \mathbf{M}^{-1}(\mathbf{k} + \mathbf{D}\gamma_k)$  is used as  $\gamma_k$  approaches  $\gamma^*$  via an iterative scheme. In [14], Nesterov developed a gradient-descent method with an improved convergence rate of  $\mathcal{O}(1/k^2)$ . In fact, the method in [14] was shown to be an ‘optimal’ first-order method for smooth problems [15] in terms of its performance among all first-order methods, up to a constant.

The following set of equations represents one iteration of the accelerated gradient descent (AGD) scheme with iterative refinement [16]. Note that  $\mathbf{y}_0 = \mathbf{x}_0 \in \mathbb{R}^n$ ,  $\theta_0 = 1$ ,  $q \in [0, 1]$  is a tuning parameter, and  $t_k$  is the step size for the current iteration.

$$\mathbf{x}_{k+1} = \mathbf{y}_k - t_k \nabla f_k \quad (29)$$

$$\theta_{k+1} \text{ solves } \theta_{k+1}^2 = (1 - \theta_{k+1}) \theta_k^2 + q \theta_{k+1} \quad (30)$$

$$\beta_{k+1} = \frac{\theta_k (1 - \theta_k)}{\theta_k^2 + \theta_{k+1}} \quad (31)$$

$$\mathbf{y}_{k+1} = \mathbf{x}_{k+1} + \beta_{k+1} (\mathbf{x}_{k+1} - \mathbf{x}_k) \quad (32)$$

$$\nabla f_{k+1} = \nabla f(\mathbf{y}_{k+1}) \quad (33)$$

Assume  $f(\mathbf{x})$  is convex and Lipschitz continuous with constant  $L$ ; i.e.,  $\|\nabla f(\mathbf{x}) - \nabla f(\mathbf{y})\|_2 \leq L\|\mathbf{x} - \mathbf{y}\|_2, \forall x, y \in \mathbb{R}^n$ . Then, the method described by Eqs. 29 through 32 converges for any  $t_k \leq 1/L$ . In the above, note that  $q = 1$  leads to  $\theta_k = 1$ ,  $\beta_k = 0$ , and  $\mathbf{y}_k = \mathbf{x}_k$  for all  $k \geq 0$ , which reduces to the gradient descent method. In general, the parameter  $q$  can tune the performance of the method depending on the specifics of the objective function  $f(\mathbf{x})$ . For example, if  $f(\mathbf{x})$  is also strongly convex, i.e.,  $\exists \mu > 0 : f(\mathbf{x}) \geq f(\mathbf{x}^*) + (\mu/2)\|\mathbf{x} - \mathbf{x}^*\|_2^2, \forall \mathbf{x} \in \mathbb{R}^n$ , then the optimal value is  $q = \mu/L$ , which achieves a linear convergence rate. If the objective function is not strongly convex, or the strong convexity parameter  $\mu$  is unknown, then it is often assumed that  $q = 0$ . Note that the original statement of the accelerated method in [14] had  $q = 0$ , so the convergence rate of  $\mathcal{O}(1/k^2)$  is still valid.

The AGD scheme can be extended to constrained optimization by ensuring that Eq. 29 does not leave the feasible set. The resulting algorithm, called Accelerated Projected Gradient Descent (APGD) can be expressed by the following set of computations to be performed at each iteration  $k \geq 0$ . Once again, let  $\mathbf{y}_0 = \mathbf{x}_0 \in \mathbb{R}^n$ , and  $\theta_0 = 1$ .

$$\mathbf{x}_{k+1} = \Pi_C(\mathbf{y}_k - t_k \nabla f_k) \quad (34)$$

$$\theta_{k+1} \text{ solves } \theta_{k+1}^2 = (1 - \theta_{k+1}) \theta_k^2 \quad (35)$$

$$\beta_{k+1} = \frac{\theta_k(1 - \theta_k)}{\theta_k^2 + \theta_{k+1}} \quad (36)$$

$$\mathbf{y}_{k+1} = \mathbf{x}_{k+1} + \beta_{k+1} (\mathbf{x}_{k+1} - \mathbf{x}_k) \quad (37)$$

$$\nabla f_{k+1} = \nabla f(\mathbf{y}_{k+1}) \quad (38)$$

When  $f(\mathbf{x})$  is convex and Lipschitz continuous with constant  $L$ , then the method described by Eqs. 34 through 37 converges for any  $t_k \leq 1/L$ . An equivalent algorithm was proved in [17] to converge with the same  $\mathcal{O}(1/k^2)$  rate as the AGD method. These computations are performed until the residual,  $r$ , which is defined as

$$r = \|\mathbf{f}\|_2, \mathbf{f} = \frac{1}{g_d} (\gamma - \Pi_K(\gamma - g_d(\mathbf{N}\gamma + \mathbf{r}))) \in \mathbb{R}^{3N_c}, \quad (39)$$

drops below a specified tolerance. This termination criteria is a scaled version of the projected gradient, and is designed to ensure that the computed projected gradient direction is tangent to the constraint manifold at the current iterate. This is desirable because it is known that at the optimal solution, the gradient is orthogonal to the constraint manifold. Therefore, it is logical to use the component of the gradient which is tangent to the constraint manifold as a measure of error. To understand this residual, first note that if  $\gamma = \gamma^*$  is optimal, then  $\Pi_K(\gamma^* - g_d(\mathbf{N}\gamma^* + \mathbf{r})) = \gamma^*$ , so  $\mathbf{f} = \mathbf{0}$  and  $r = 0$  as expected. Second, consider the case when  $\gamma$  is not optimal. Then, it can be verified that

$$\Pi_K(\gamma - g_d(\mathbf{N}\gamma + \mathbf{r})) = \gamma - g_d\mathbf{f}. \quad (40)$$

In the preceding, the left hand side is equivalent to taking a step of length  $g_d$  in the negative gradient direction and projecting back to the feasible region. The right hand side says that the same point can be reached by taking a step of length  $g_d$  in the direction opposite of  $\mathbf{f}$ . In the limit, as  $g_d \rightarrow 0$ , the direction  $\mathbf{f}$  approaches the plane tangent to the constraint manifold. Note that  $r$  could be used to measure convergence for any value of  $g_d$ , but a small value was used in practice for the reasons just stated.

### 2.3. The anti-relaxed APGD algorithm

This section states the overall algorithm obtained when applying the APGD method with anti-relaxation to the problem in Eq. 15. As stated, the algorithm includes an adaptive step size which may both shrink and grow, an adaptive restart scheme based on the gradient, and a fall-back strategy to allow early termination [12].

ALGORITHM APGD WITH ANTI-RELAXATION( $\mathbf{N}$ ,  $\mathbf{r}$ ,  $\tau$ ,  $N_{max}$ )

$$(1) \quad \gamma_0 = \mathbf{0}_{n_c}$$

$$(2) \quad \hat{\gamma}_0 = \mathbf{1}_{n_c}$$

$$(3) \quad \mathbf{y}_0 = \gamma_0$$

$$(4) \quad \mathbf{r}_0 = \mathbf{r}$$

$$(5) \quad \theta_0 = 1$$

$$(6) \quad L_k = \frac{\|\mathbf{N}(\gamma_0 - \hat{\gamma}_0)\|_2}{\|\gamma_0 - \hat{\gamma}_0\|_2}$$

$$(7) \quad t_k = \frac{1}{L_k}$$

$$(8) \quad \text{for } k := 0 \text{ to } N_{max}$$

$$(9) \quad \mathbf{g} = \mathbf{N}\mathbf{y}_k + \mathbf{r}$$

$$(10) \quad \gamma_{k+1} = \Pi_K(\mathbf{y}_k - t_k \mathbf{g})$$

$$(11) \quad \text{while } \frac{1}{2} \gamma_{k+1}^T \mathbf{N} \gamma_{k+1} + \gamma_{k+1}^T \mathbf{r} \geq \frac{1}{2} \mathbf{y}_k^T \mathbf{N} \mathbf{y}_k + \mathbf{y}_k^T \mathbf{r} + \mathbf{g}^T (\gamma_{k+1} - \mathbf{y}_k) + \frac{1}{2} L_k \|\gamma_{k+1} - \mathbf{y}_k\|_2^2$$

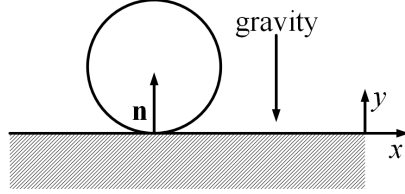


Figure 1: Sphere on a fixed horizontal plane.

```

(12)       $L_k = 2L_k$ 
(13)       $t_k = \frac{1}{L_k}$ 
(14)       $\gamma_{k+1} = \Pi_K(\mathbf{y}_k - t_k g)$ 
(15)      endwhile
(16)       $\theta_{k+1} = \frac{-\theta_k^2 + \theta_k \sqrt{\theta_k^2 + 4}}{2}$ 
(17)       $\beta_{k+1} = \theta_k \frac{1 - \theta_k}{\theta_k^2 + \theta_{k+1}}$ 
(18)       $\mathbf{y}_{k+1} = \gamma_{k+1} + \beta_{k+1} (\gamma_{k+1} - \gamma_k)$ 
(19)       $r = r(\gamma_{k+1})$ 
(20)      if  $r < \epsilon_{min}$ 
(21)           $r_{min} = r$ 
(22)           $\hat{\gamma} = \gamma_{k+1}$ 
(23)      endif
(24)      if  $r < \tau$ 
(25)          break
(26)      endif
(27)      if  $\mathbf{g}^T(\gamma_{k+1} - \gamma_k) > 0$ 
(28)           $\mathbf{y}_{k+1} = \gamma_{k+1}$ 
(29)           $\theta_{k+1} = 1$ 
(30)      endif
(31)       $L_k = 0.9L_k$ 
(32)       $t_k = \frac{1}{L_k}$ 
(33)       $\mathbf{v}_k = \mathbf{M}^{-1}(\mathbf{k} + \mathbf{D}\gamma_{k+1})$ 
(34)      for  $i = 1$  to  $n_c$ 
(35)           $\lambda_i = \sqrt{(\mathbf{D}_{i,u}^T \mathbf{v}_k)^2 + (\mathbf{D}_{i,w}^T \mathbf{v}_k)^2}$ 
(36)           $\mathbf{r} = \mathbf{r}_0$ 
(37)           $\mathbf{r}_{i,n} = \mathbf{r}_{i,n} + \lambda_i \mu_i$ 
(38)      endfor
(39)      return Value at time step  $t_{l+1}$ ,  $\gamma^{l+1} := \hat{\gamma}$  .

```

### 3. Numerical experiments

This section analyzes the effect of anti-relaxation using three different numerical experiments. The first numerical experiment in §3.1 thoroughly analyzes the simple case of a sphere transitioning from pure sliding to rolling. The second experiment in §3.2 investigates the effect of anti-relaxation over time for a filling test with 1000 spheres. The last experiment in §3.4 looks at several filling tests, each with a different number of bodies, to investigate the effect of the anti-relaxation as a function of the number of collisions.

#### 3.1. A 2D example

The first numerical experiment thoroughly analyzes the dynamics of a 3D ball (two translational and one rotational degrees of freedom,  $\mathbf{q} = [q_x, q_y, \omega]^T \in \mathbb{R}^3$ ) as it transitions from pure sliding to rolling [18]. In this case,  $\gamma = [\gamma_n, \gamma_t]^T \in \mathbb{R}^2$  because there is only a normal and tangential impulse. Fig. 1 shows an

elevation view of a rough uniform sphere of unit radius and mass in contact with a fixed horizontal plane in a uniform gravitational field. This example was chosen because of the existence of an easily obtainable closed-form solution of the dynamic motion of the sphere for certain conditions. Let the plane coincide with the  $xz$ -plane of a (right-handed) inertial frame, with the inertial  $y$ -direction upward. Thus, there will be a single contact with the  $\mathbf{n}$  always pointed in the  $y$ -direction, the  $\mathbf{u}$  always pointed in the  $x$ -direction (there is no  $\mathbf{w}$  in this example), and the gap function  $\Phi = q_y - 1$  so that  $\mathbf{b} = [\frac{1}{h}(q_y - 1), 0]^T \in \mathbb{R}^2$ . The coefficient of friction was assumed to have a constant value of 0.2. The matrices  $\mathbf{D}$  and  $\mathbf{M}$  can be seen to be constant throughout the motion. For this problem, the various matrices are:

$$\mathbf{M} = \begin{bmatrix} 1 & 0 & 0 \\ 0 & 1 & 0 \\ 0 & 0 & 0.4 \end{bmatrix} \quad (41)$$

$$\mathbf{D} = \begin{bmatrix} 0 & 1 \\ 1 & 0 \\ 0 & 1 \end{bmatrix} \quad (42)$$

$$\mathbf{f}_{\text{ext}} = \begin{bmatrix} 0 \\ -9.81 \\ 0 \end{bmatrix} \quad (43)$$

Given the following initial conditions:

$$\mathbf{q}_0 = [0 \ 1 \ 0]^T \quad (44)$$

$$\mathbf{v}_0 = [2 \ 0 \ 0]^T, \quad (45)$$

using  $h = 0.01$  s the matrices  $\mathbf{N}$  and  $\mathbf{r}$  can be calculated from Eqs. 12 and 13 and will result in:

$$\mathbf{N} = \begin{bmatrix} 1 & 0 \\ 0 & 3.5 \end{bmatrix} \quad (46)$$

$$\mathbf{r} = \begin{bmatrix} -0.0981 \\ 2 \end{bmatrix} \quad (47)$$

The sphere initially slides in the  $x$ -direction, gathering angular velocity until the transition time,  $t_{trn} = \frac{2v_{x_0}}{7g\mu} \approx 0.291$  s where  $v_{x_0}$  is the initial velocity in the  $x$ -direction and  $g = 9.81 \text{ m s}^{-2}$ . After the transition time, the sphere rolls with constant velocity in the  $x$ -direction and angular velocity  $\omega = \frac{5v_{x_0}}{7} \approx 1.429 \text{ m s}^{-1}$ . The analytical solution for the contact impulses at  $t = 0$  s can be shown to be  $\gamma_{\text{analytical}} = [0.0981, -0.01962]^T$ . Although the anti-relaxed method matched the analytical solution, shown in Fig. 2, using the relaxed CCQO of Eq. 14 results in incorrect behavior, even at the initial time step.

To graphically understand the non-physical behavior that is occurring at  $t = 0$ , four situations have been plotted in Figs. 3-6. Fig. 3 represents the original DVI that must be solved at  $t = 0$  plotted in the  $\gamma_n$ - $\gamma_t$  domain by substituting the velocity terms for contact impulses using Eq. 7. The contours, shown by the colored lines, represent the objective function in Eq. 4, the cone constraints of which are shown by the solid black lines (the solution must lie in the interior of these lines). Lastly, the complementarity condition in Eq. 8 is captured by the dotted and dashed lines. If  $\gamma_n = 0$ , then  $\gamma_t$  must lie on the dashed line; if  $\gamma_n$  is nonzero, the solution must lie on the dotted line. The optimum and analytical solutions are indicated by the red  $X$  and circle, respectively. As this is the true DVI, the optimum and analytical solutions match. Fig. 4 shows what happens when Eq. 8 is replaced with the relaxed complementarity condition in Eq. 10. The complementarity condition associated with normal velocities bifurcates, resulting in the optimum being increased in magnitude. Physically, this would result in the ball being launched off of the ground. The relaxed CCQO of Eq. 14 is shown in Fig. 5. Here the contours represent the quadratic objective function and the solid black lines represent the conic constraints (the solution must lie in the interior of these lines).

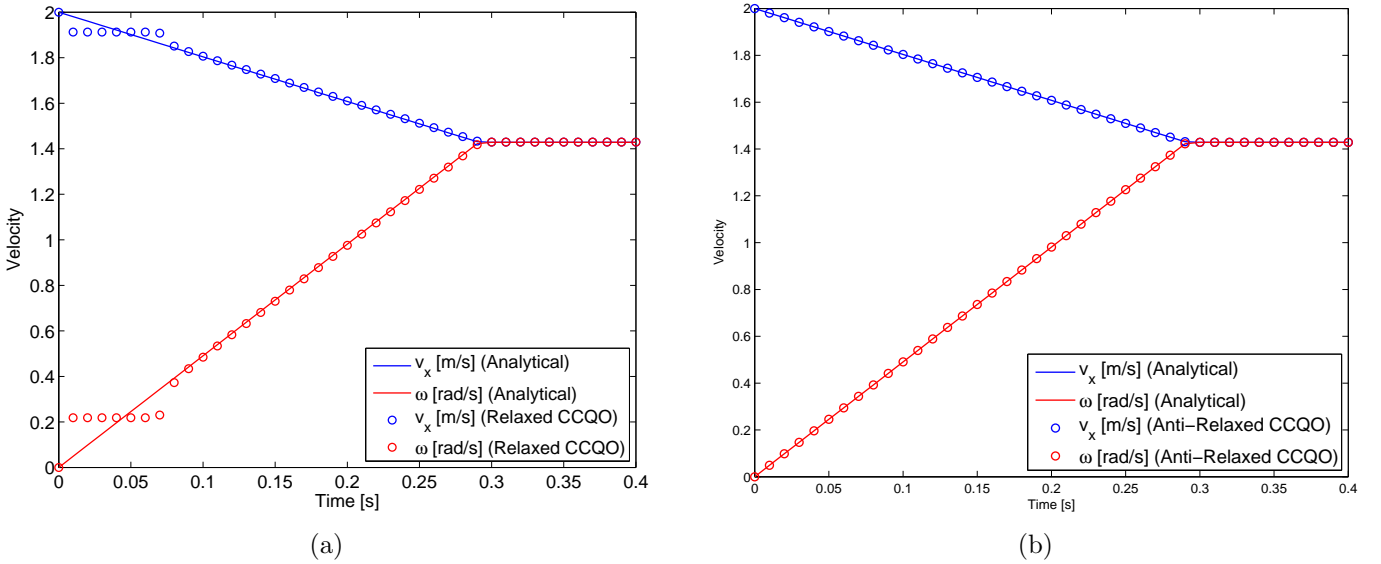


Figure 2: Rolling ball test for the analytical and numerical velocities with the relaxed CCQO (left) and the anti-relaxed CCQO (right).

The dashed line represents the non-negativity constraint on  $\gamma_n$  - the solution must lie on or to the right of this line. Since the relaxed CCQO is equivalent to the relaxed DVI/CCP, the optimum (represented by the red circle) will be identical to the one in Fig. 4. Notice that, like the relaxed DVI/CCP, the optimum does not match the analytical solution to the problem. Lastly, using anti-relaxation from Eq. 15 results in a shift of the contours of the objective function in the negative  $\gamma_n$ -direction. This shift results in an optimum that coincides with the analytical solution. Additional surface plots of the objective functions and constraints can be viewed in Appendix A.

### 3.2. Filling test

The second numerical experiment studies a model of spherical bodies falling into a container under gravity, the time evolution of which can be seen in Fig. 7. The goal of this study was to see how anti-relaxation effects the physical results of the simulation. Several statistics were monitored, such as the computation time, number of iterations performed at each step, maximum velocity of the bodies, and contact force on the container. In this case, there are 1000 spheres, each with a radius  $r = 1$  m, mass  $m = 1$  kg, and friction coefficient  $\mu = 0.25$ . The system had a gravitational acceleration in the vertical direction  $g = 9.81 \text{ m s}^{-1}$ . The simulation was run for 5 s with a time step  $h = 0.01$  s and a solver tolerance of  $\tau = 0.00001 \text{ g cm s}^{-1}$ .

The results of the simulation are plotted in Fig. 8. Fig. 8a shows the total contact force that the container experiences as a function of time. The dynamics behavior as determined by the relaxed CCQO (using Eq. 14) is represented by the blue line and dynamics behavior as determined by the anti-relaxed CCQO (using Eq. 15) is represented by the red line. Although both models converge to the total weight of the spheres, the dynamics are clearly different and the anti-relaxed solution settles much sooner than the relaxed solution. The complementarity error in the anti-relaxed solution, calculated using Eq. 8 and shown in Fig. 8b, is several orders of magnitude less than the relaxed solution.

### 3.3. Compaction test

The third numerical experiment studies a model of spherical bodies in a container being compacted by a slab, the time evolution of which can be seen in Fig. 9. The goal of this study was to see how anti-relaxation effects the physical results of the simulation. Several statistics were monitored, such as the computation time, number of iterations performed at each step, and contact force on the container. In this case, there are 1000 spheres, each with a radius  $r = 1$  m, mass  $m = 1$  kg, and friction coefficient  $\mu = 0.25$ . The upper slab prevents spheres from escaping the container and has a mass  $m = 4000$  kg and friction coefficient  $\mu = 0.25$ .

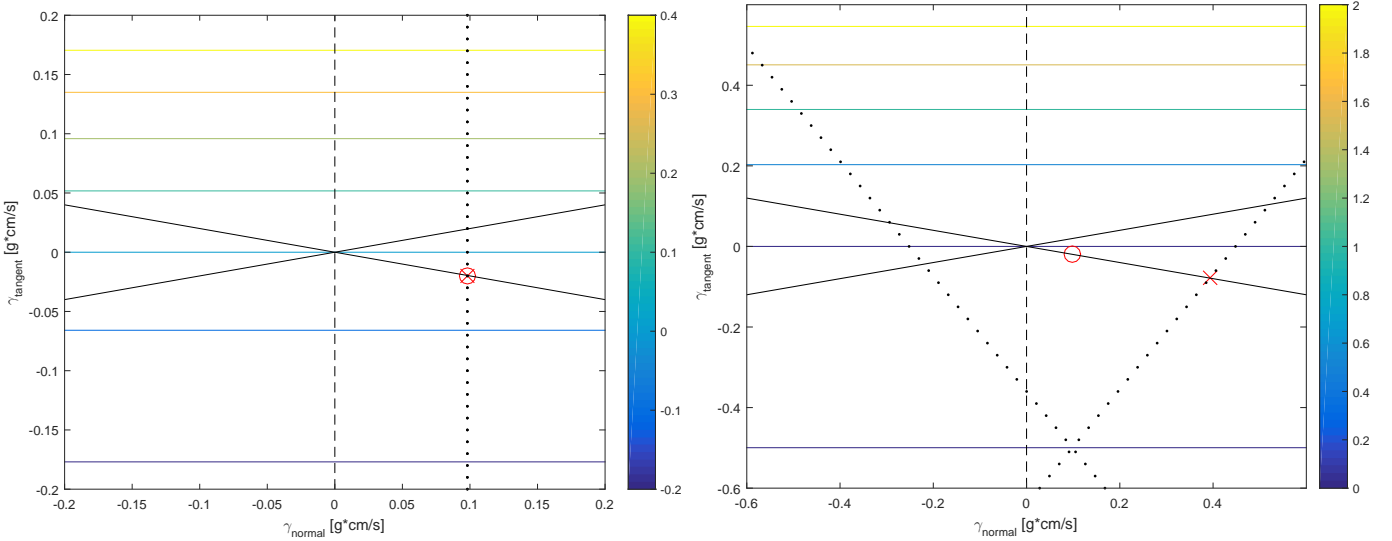


Figure 3: The original DVI problem based on Eqs. 6-9.

Figure 4: The relaxed DVI/CCP problem based on Eq. 10.

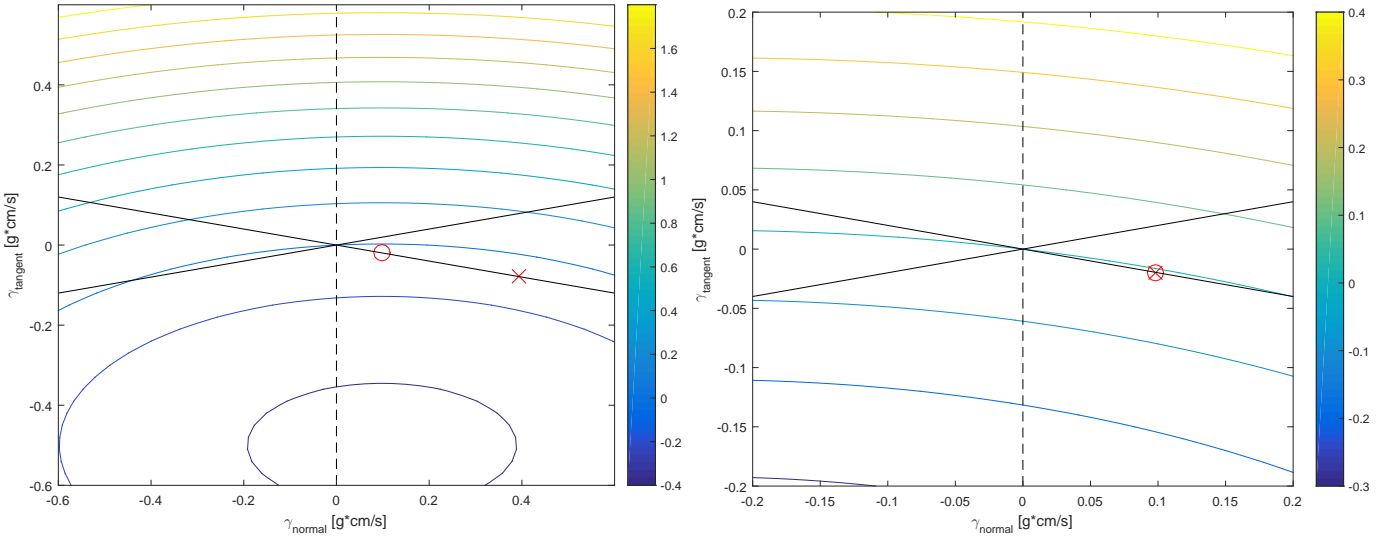


Figure 5: The relaxed CCQO based on Eq. 14.

Figure 6: The anti-relaxed CCQO based on Eq. 15.

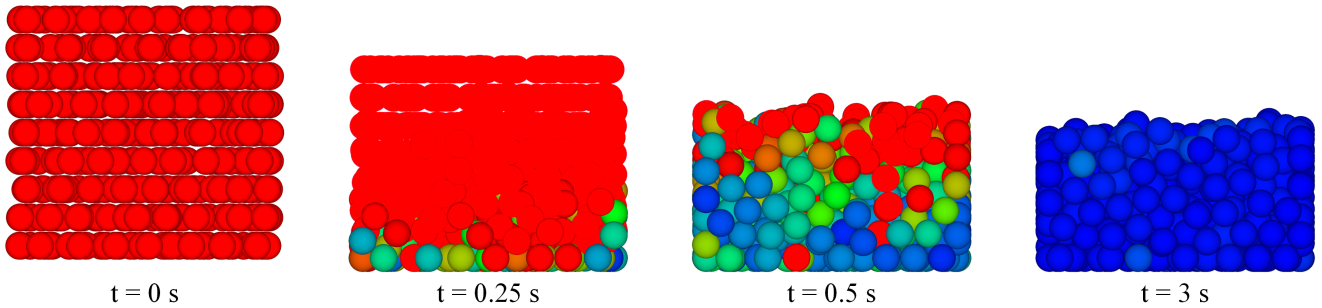


Figure 7: A simulation of 1000 spherical bodies falling into a container due to gravity. The colors of the bodies represent the magnitude of the linear velocity (red = fast, blue = slow).

The system has a gravitational acceleration in the vertical direction  $g = 9.81 \text{ m s}^{-1}$ . The simulation was run for 4 s with a time step  $h = 0.001 \text{ s}$  and a solver tolerance of  $\tau = 0.00001 \text{ g cm s}^{-1}$ .

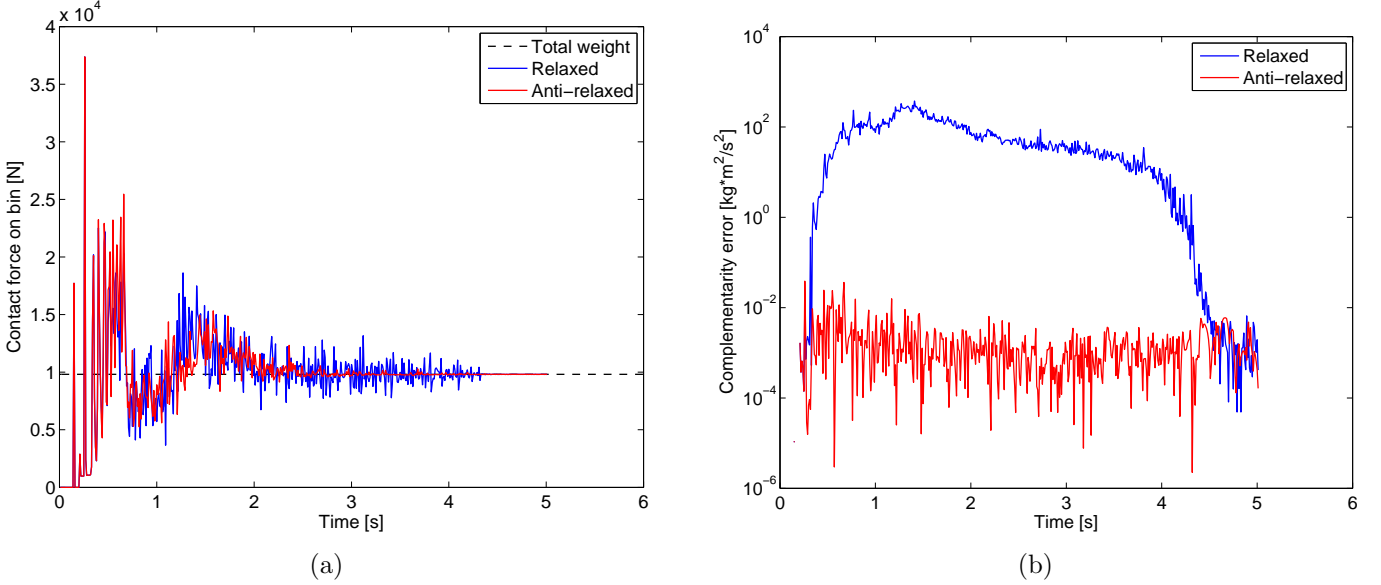


Figure 8: Simulation of the contact force experienced by the container (left) and the complementarity error (right) as a function of time.

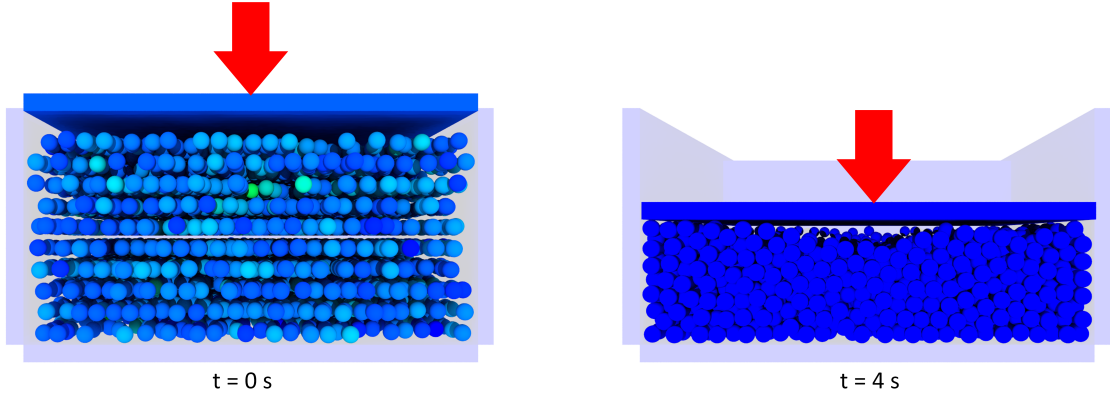


Figure 9: A simulation of 4000 spherical bodies in a container being compacted by a slab. The colors of the bodies represent the magnitude of the linear velocity (red = fast, blue = slow).

The results of the simulation are plotted in Fig. 10. Fig. 10a shows the total contact force that the container experiences as a function of time. The dynamics behavior as determined by the relaxed CCQO (using Eq. 14) is represented by the blue line and dynamics behavior as determined by the anti-relaxed CCQO (using Eq. 15) is represented by the red line. Although both models converge to the total weight of the spheres and slab, the dynamics are clearly different and the anti-relaxed solution settles much sooner than the relaxed solution. The complementarity error in the anti-relaxed solution, calculated using Eq. 8 and shown in Fig. 10b, is several orders of magnitude less than the relaxed solution.

### 3.4. Scaling analysis

The last numerical experiment studies several models of spherical bodies falling into a container under gravity to understand how the solver statistics change as a function of the number of collisions. Several statistics were monitored, such as the computation time, number of iterations performed at each step, maximum velocity of the bodies, and contact force on the container. The number of spheres is varied from 10 to 16 000, each with a radius  $r = 1\text{ m}$ , mass  $m = 1\text{ kg}$ , and friction coefficient  $\mu = 0.25$ . The system had a gravitational acceleration in the vertical direction  $g = 9.81\text{ m s}^{-1}$ . Each simulation was run for 5 s with a

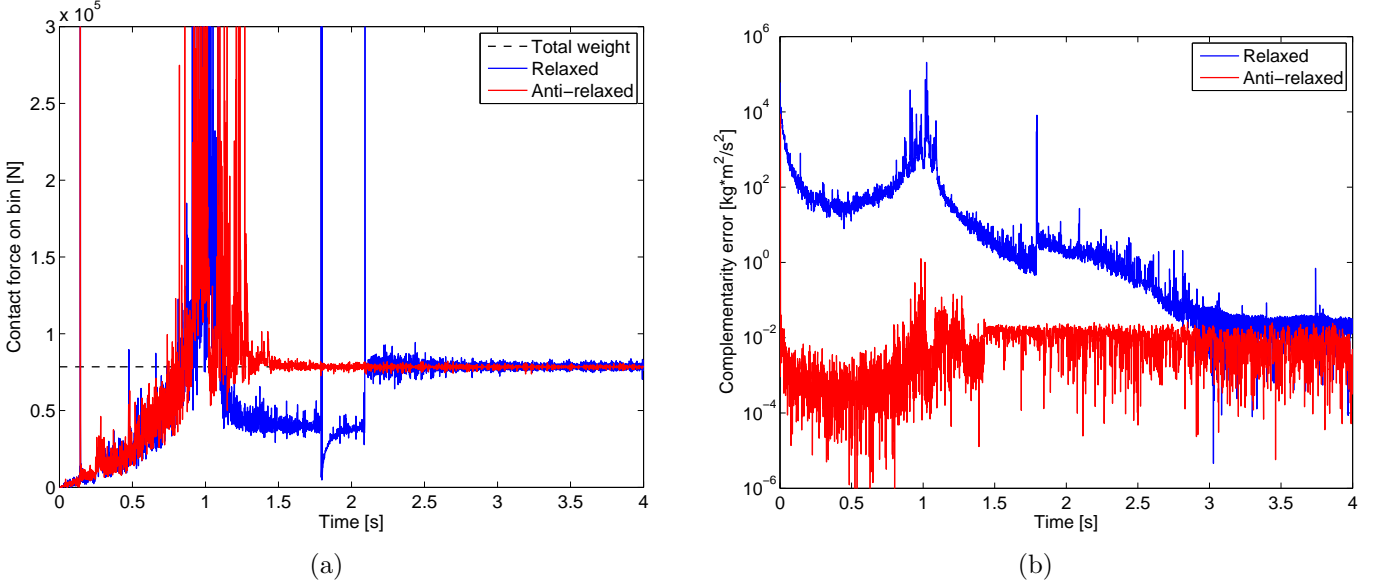


Figure 10: Simulation of the contact force experienced by the container (left) and the complementarity error (right) as a function of time.

time step  $h = 0.01$  s and a solver tolerance of  $\tau = 0.000\,01 \text{ g cm s}^{-1}$ .

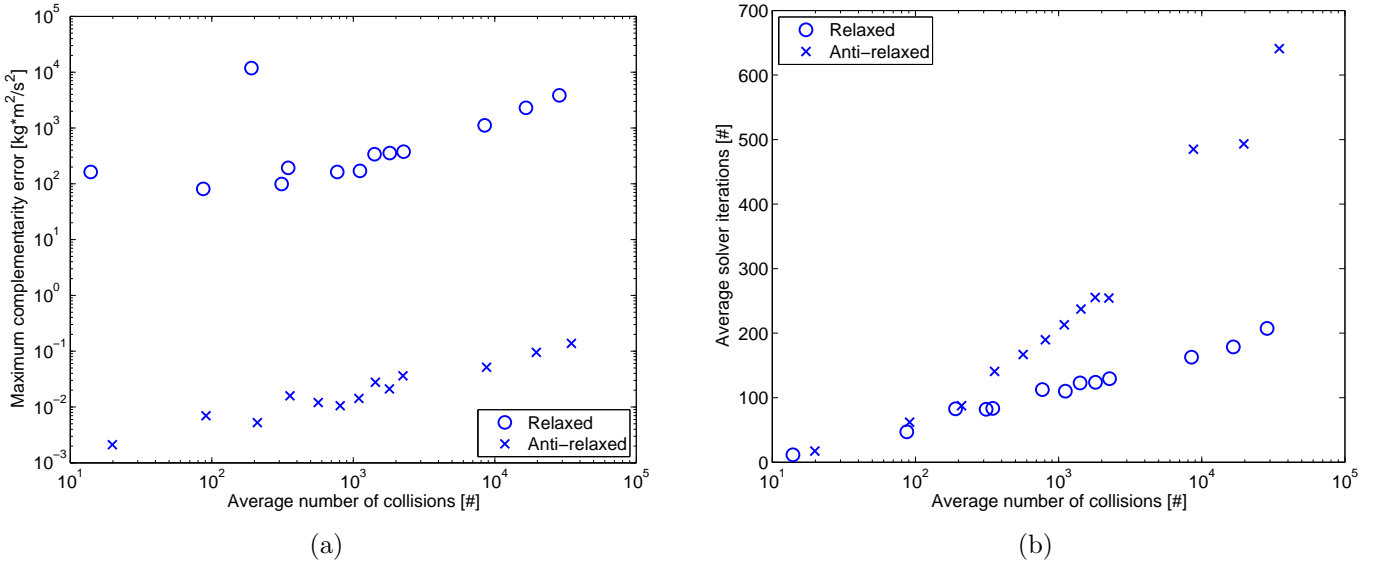


Figure 11: The maximum complementarity error (left) and the average number of iterations (right) as a function of the number of collisions.

The results of the simulation are plotted in Fig. 11. Fig. 11a shows the maximum complementarity error (calculated using Eq. 8) that occurs over the entire simulation. It is important to note that the complementarity error in both models increases as the number of collisions increases, although the error in the anti-relaxed solution is again several orders of magnitude lower than the relaxed solution. Fig. 11b shows the average number of APGD iterations that are used to solve the CCQO over the entire simulation. Although the number of iterations are similar for low numbers of collisions (below 100 spheres), the anti-relaxed solution quickly becomes increasingly costly as the number of collisions increases.

#### 4. Summary and conclusions

This paper summarizes an approach for predicting the position and velocity evolution of a group of rigid particles that are subject to non-interpenetration, collision, adhesion, and dry friction constraints and to possibly global forces (such as electrostatic and gravitational forces). The DVI model is based on complementarity conditions for contact and differential inclusions for handling friction forces. By adding a term to mathematically relax the DVI, the model can be posed as a CCP and the solution can be found by solving a CCQO. In many cases, the relaxation results in non-physical behavior. In this work, the objective function of the CCQO is modified by an anti-relaxation term to result in a solution that is equivalent to the optimum of the original DVI. Three numerical experiments were carried out to analyze the effect of anti-relaxation. The first numerical experiment thoroughly analyzed the simple case of a sphere transitioning from pure sliding to rolling and described in graphical form the error that relaxation can introduce. The second experiment investigated the effect of anti-relaxation over time for a filling test with 1000 spheres. It was determined that the anti-relaxation results in less noise, or “jitter”, in the settled configuration and results in a complementarity error that is several orders of magnitude lower than the relaxed solution. The last experiment looked at several filling tests, each with a different number of bodies, to investigate the effect of the anti-relaxation as a function of the number of collisions. It was found that the number of iterations are similar for low numbers of collisions (below 100 spheres) but the anti-relaxed solution quickly becomes increasingly costly as the number of collisions increases.

#### References

- [1] E. J. Haug, Computer-Aided Kinematics and Dynamics of Mechanical Systems Volume-I, Prentice-Hall, Englewood Cliffs, New Jersey, 1989.
- [2] A. A. Shabana, Dynamics of Multibody Systems, 4th Edition, Cambridge University Press, Cambridge, England., 2013.
- [3] M. Anitescu, F. A. Potra, Formulating dynamic multi-rigid-body contact problems with friction as solvable linear complementarity problems, *Nonlinear Dynamics* 14 (1997) 231–247.
- [4] J.-S. Pang, D. Stewart, Differential variational inequalities, *Mathematical Programming* 113 (2) (2008) 345–424.
- [5] M. Anitescu, Optimization-based simulation of nonsmooth rigid multibody dynamics, *Mathematical Programming* 105 (1) (2006) 113–143. doi:<http://dx.doi.org/10.1007/s10107-005-0590-7>.
- [6] G. Daviet, F. Bertails-Descoubes, L. Boissieux, A hybrid iterative solver for robustly capturing coulomb friction in hair dynamics, in: *ACM Transactions on Graphics (TOG)*, Vol. 30 (6), ACM, 2011, p. 139.
- [7] D. E. Stewart, Rigid-body dynamics with friction and impact, *SIAM Review* 42(1) (2000) 3–39.
- [8] D. Baraff, Fast contact force computation for nonpenetrating rigid bodies, in: *Computer Graphics (Proceedings of SIGGRAPH)*, 1994, pp. 23–34.
- [9] A. Tasora, A fast NCP solver for large rigid-body problems with contacts, in: C. Bottasso (Ed.), *Multibody Dynamics: Computational Methods and Applications*, Springer, 2008, pp. 45–55.
- [10] M. Anitescu, A. Tasora, An iterative approach for cone complementarity problems for nonsmooth dynamics, *Computational Optimization and Applications* 47 (2) (2010) 207–235. doi:[10.1007/s10589-008-9223-4](https://doi.org/10.1007/s10589-008-9223-4).
- [11] A. Tasora, M. Anitescu, A matrix-free cone complementarity approach for solving large-scale, non-smooth, rigid body dynamics, *Computer Methods in Applied Mechanics and Engineering* 200 (5-8) (2011) 439–453. doi:[doi:10.1016/j.cma.2010.06.030](https://doi.org/10.1016/j.cma.2010.06.030).

- [12] T. Heyn, On the Modeling, Simulation, and Visualization of Many-Body Dynamics Problems with Friction and Contact, PhD thesis, Department of Mechanical Engineering, University of Wisconsin–Madison, [http://sbel.wisc.edu/documents/TobyHeynThesis\\_PhDfinal.pdf](http://sbel.wisc.edu/documents/TobyHeynThesis_PhDfinal.pdf) (2013).
- [13] F. Cadoux, An optimization-based algorithm for coulomb's frictional contact, *ESAIM: Proc.* 27 (2009) 54–69. doi:10.1051/proc/2009019.  
URL <http://dx.doi.org/10.1051/proc/2009019>
- [14] Y. Nesterov, A method of solving a convex programming problem with convergence rate  $\mathcal{O}(1/k^2)$ , in: *Soviet Mathematics Doklady*, Vol. 27(2), 1983, pp. 372–376.
- [15] A. Nemirovsky, D. B. Yudin, *Problem complexity and method efficiency in optimization.*, John Wiley & Sons, 1983.
- [16] Y. Nesterov, *Introductory lectures on convex optimization: A basic course*, Vol. 87, Springer, 2003.
- [17] A. Beck, M. Teboulle, A fast iterative shrinkage-thresholding algorithm for linear inverse problems, *SIAM Journal on Imaging Sciences* 2 (1) (2009) 183–202.
- [18] J. C. Trinkle, Formulation of Multibody Dynamics as Complementarity Problems, Volume 5: 19th Biennial Conference on Mechanical Vibration and Noise, Parts A, B, and C 2003 (2003) 361–370. doi:10.1115/DETC2003/VIB-48342.  
URL <http://proceedings.asmedigitalcollection.asme.org/proceeding.aspx?articleid=1587646>

# Appendices

## A. Additional plots

### A.1. Surface plots of the objective functions

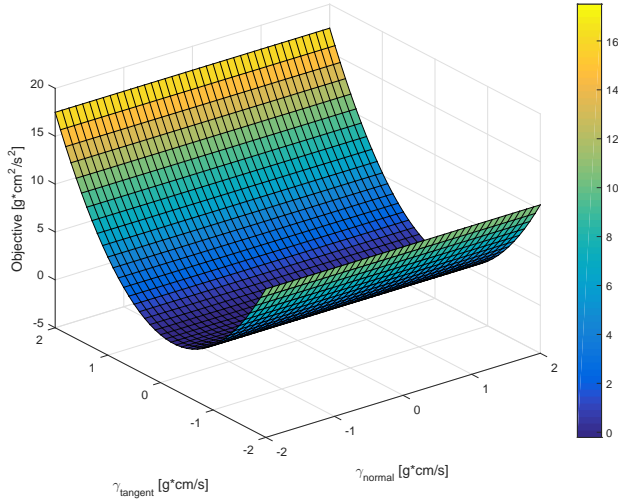


Figure 12: The original DVI problem based on Eqs. 6-9.

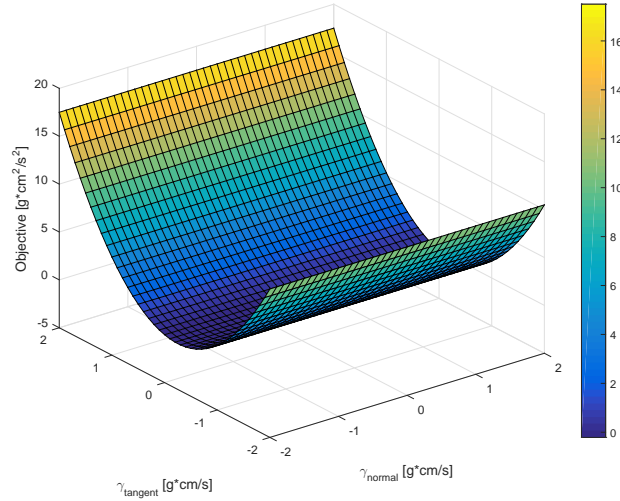


Figure 13: The relaxed DVI/CCP problem based on Eq. 10.

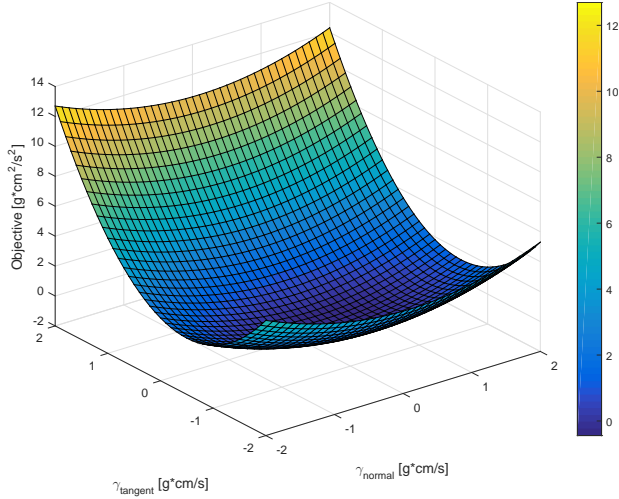


Figure 14: The relaxed CCQO based on Eq. 14.

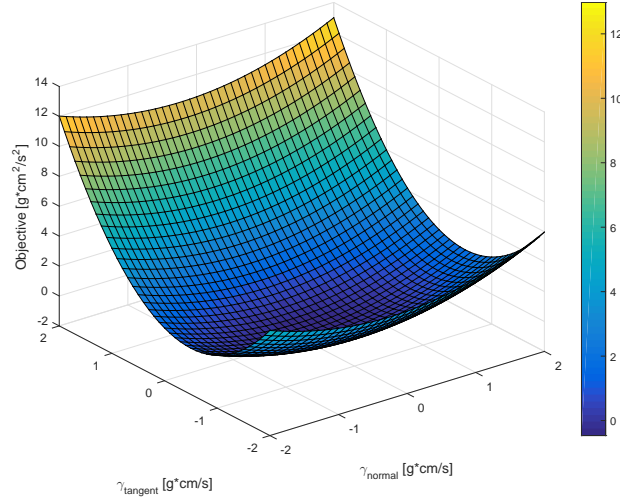


Figure 15: The anti-relaxed CCQO based on Eq. 15.

### A.2. Constraint plots with objective contours

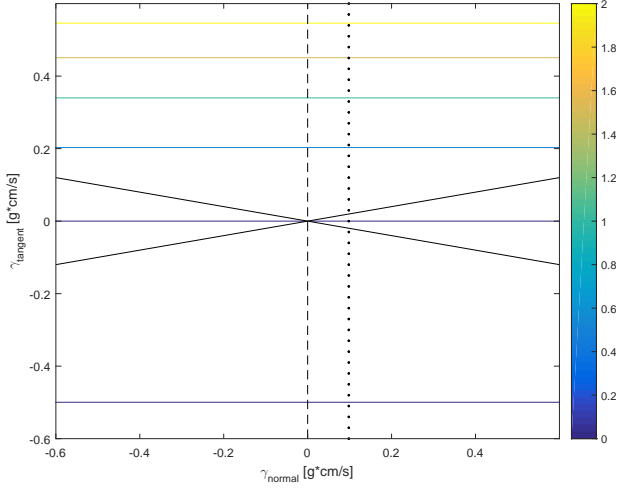


Figure 16: The original DVI problem based on Eqs. 6-9.

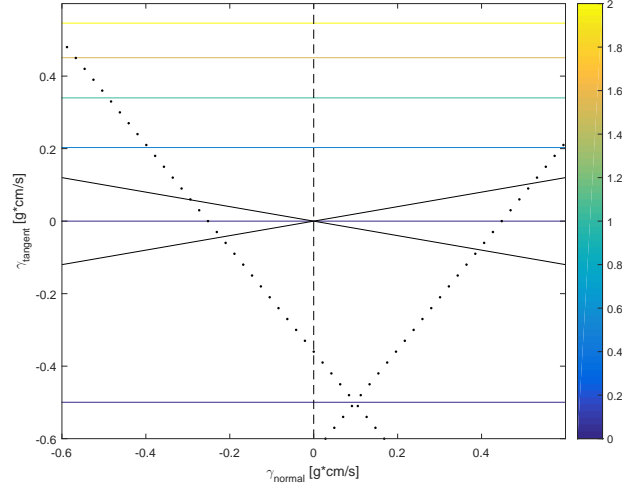


Figure 17: The relaxed DVI/CCP problem based on Eq. 10.

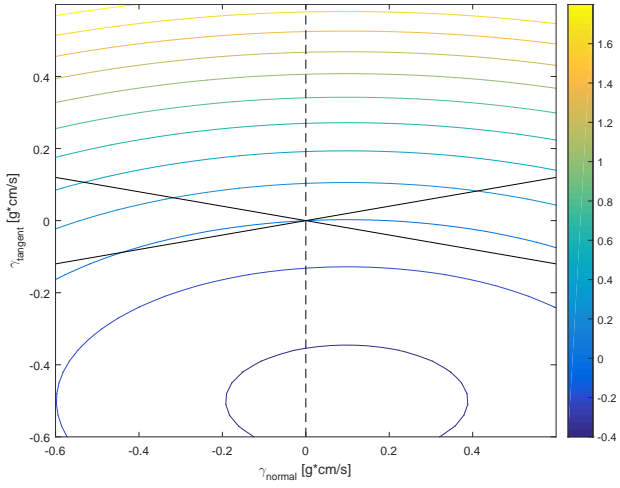


Figure 18: The relaxed CCQO based on Eq. 14.

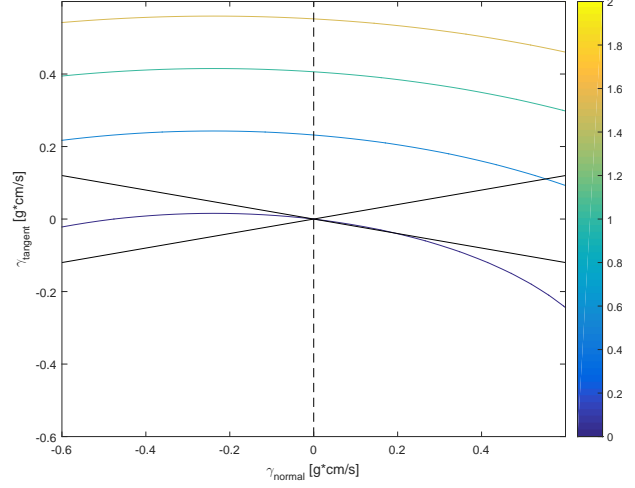


Figure 19: The anti-relaxed CCQO based on Eq. 15.